THE KEY TECHNOLOGIES OF GEOLOGICAL DISASTER DYNAMIC MONITORING BASED ON NAP-OF-THE-OBJECT PHOTOGRAMMETRY

Yinghang Wang[1], Yansong Duan[1,]*, Bohui Pang[2], Ruixiang Liu[1]

[1]School of Remote Sensing and Information Engineering, Wuhan University, Wuhan 430079, yh_wang@whu.edu.cn, ysduan@whu.edu.cn, lrx_lucky@whu.edu.cn
[2]Huaneng Lancang River Hydropower INC, pangbohui@lcjgs.chng.com.cn

KEY WORDS: Geologic Hazard, Dynamic Monitoring, Nap-of-the-object Photogrammetry, Refined 3D model

ABSTRACT:

Dynamic monitoring of geological hazards is an important project. Photogrammetry plays an important role in geological hazard monitoring, because of its advantages of convenient data processing, low cost, non-contact, direct texture information and intricate 3-D real scene model. For the traditional photogrammetry can not meet the needs of dynamic monitoring, based on multi-period nap-of-the-object photogrammetry, this paper obtains high-precision images and produces a refined 3D real scene model to carry out the dynamic monitoring of geological disasters. A deformation detection method of geological hazards based on the comparison of three-dimensional model differences is proposed to locate the position with serious deformation. Then, based on the severely deformed area, the multi-period generalized orthophotos are produced, and the image feature matching is used to find the homonymous points between the generalized orthophotos. The two-dimensional and three-dimensional coordinate forward and inverse transformation of the generalized orthophotos are used to calculate the size and direction of the deformation displacement, analyze the deformation trend of geological disasters, and finally realize accurate monitoring of the deformation trend of geological disasters. The results show that the deformation area detection method proposed in this paper is simple and effective, which can quickly find the deformation position. The deformation trend prediction based on multi-period generalized orthophotos is feasible, and the displacement with deformation of 3CM can be accurately pointed out.

1. INTRODUCTION

At present, geological disasters occur frequently around the world and have a huge impact on people's production and life. Geological disasters have a wide distribution range, are sudden and hidden, and are difficult to predict. In terms of monitoring geological disasters, traditional geological geography methods have problems, such as high time cost, high economic cost, single acquisition of geological information, cumbersome process, and poor timeliness (Li, 2019). In contrast, UAV photogrammetry has the advantages of wide range, low cost, high precision, great quality and rich information in monitoring (Zai, 2021). However, traditional UAV photogrammetry is affected by flight altitude and lens inclination, the details of target objects and side textures obtained by these two methods are insufficient, and the three-dimensional position and texture information provided are limited (Zhang, 2020). The " Nap-of-the-object Photogrammetry " proposed by Academician Zhang Zuxun realizes the collection of high-resolution images (sub-centimeter or even millimeter-level), which can be used in building a high-precision 3D model of landslide hazards with delicate texture, high precision and great effect (He, 2019). Based on this high-precision three-dimensional model, accurate dynamic monitoring of geological disasters can be achieved. Liang et al. studied the early identification of high-level collapse by combining Nap-of-the-object photogrammetry and multi-angle detection technology. Taking gouda mountain in Kangding County as an example, he realized the investigation and prediction of high-level collapse. Yang et al. used Nap-of-the-object photogrammetry to obtain high-precision images of the target project, which was applied to the supervision of the middle route of the South-to-North Water Transfer Project, and realized the accurate elimination of a variety of hidden dangers. Li et al. used Nap-of-the-object photogrammetry to obtain the data of the target area, realized the dynamic monitoring of terrain height through periodic difference analysis, and analysed the surface sediment erosion

status. Based on the above research, this paper proposes a key technology of geological disaster dynamic monitoring based on Nap-of-the-object photogrammetry: using Nap-of-the-object photogrammetry to collect multi-period images of the target area, produce three-dimensional digital elevation models(DEM), and establish refined 3D real scene models; Through the analysis of DEM differences in multiple periods, the deformation location of geological disasters is discovered; then, produce multi-period generalized orthophotos, extract corresponding image points by image matching, and calculate the deformation displacement vector, in order to monitor the deformation trend of geological disasters.

2. NAP-OF-THE-OBJECT PHOTOGRAMMETRY

Nap-of-the-object Photogrammetry is a new type of photogrammetry processing method, which could adapt to the fluctuation of the target surface to capture high-resolution images for the target section, taking advantage of rotor drone photography.

After acquiring ultra-high-resolution images, First, aerotriangulation is performed to achieve the orientation, and then 3D point cloud is produced through dense matching; finally, a 3D Mesh model is constructed and textures are attached to produce a refined 3D scene model.

Nap-of-the-object Photogrammetry originates from the monitoring of geological disasters and landslide. Its advantages in fine modeling have created far-reaching prospects for this technology in many fields of geology, humanities and society, such as landslide monitoring, 3D fine digitization of ancient building structures, and 3D reconstruction and management of intelligent cities, exploration and monitoring of hidden dangers of water conservancy projects.

Nap-of-the-object photogrammetry lies in two aspects: the strategy of "from scratch" and the idea of "from coarse to fine".

Based on these two core parts, the workflow of automatic collection of high-precision data for Nap-of-the-object photogrammetry is shown in Fig. 1.

---

* Corresponding author
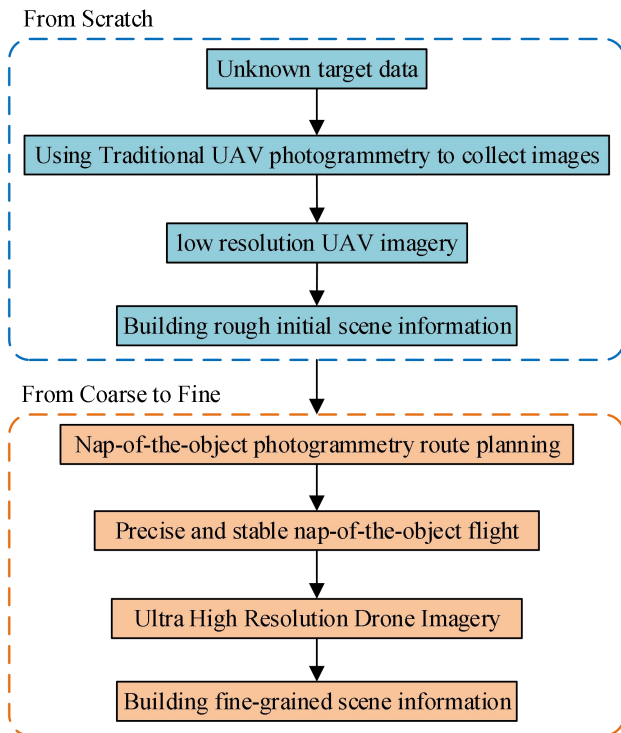
From Scratch

Figure 1. Automatic collection workflow of high-precision data for nap-of-the-object photogrammetry

In Fig.1, (1) "From scratch" refers to: first, the traditional UAV photogrammetry technology is used to collect images of unknown research targets, and to reconstruct the rough initial scene information of the research targets. (2) "From coarse to fine" refers to: designing routes through coarse models to obtain optimal high-resolution images and producing fine 3D models.

3. GEOLOGICAL DISASTER DYNAMIC MONITORING

In order to discover the location of geological deformation and monitor the trend, this paper proposes a method for dynamic monitoring of geological hazards based on Nap-of-the-object Photogrammetry: first, the multi-period images of the target area are collected by Nap-of-the-object photogrammetry, and through aerial triangulation and dense matching, dense point cloud data LAS, refined three-dimensional reality model are obtained. Then, the 3D model DEM is produced according to the preprocessing results, and the deformation of geological disasters is discovered by multi-period DEM difference analysis. Finally, multi-period generalized orthophotos are generated based on the 3D data, the corresponding image points are detected by image matching, the coordinates of the image points or 3D model points are calculated by using the forward and inverse coordinate transformation relationship between the 3D model and the 2D projection plane, and the deformation displacement vector is calculated to realize the monitoring of the deformation trend of geological disasters.The technical process of the whole method is shown in Fig.2.

The technology for establishing fine 3D models is relatively mature, and there have been a large number of research studies on this, such as (Zheng, 2005) and (Shen, 2017), which will not be discussed here, but will focus on deformation monitoring technology.

After obtaining the multi-period 3D models, in order to quantify the deformation area and deformation size, this paper adopts a two-step positioning method. First, the DEM difference analysis

is used to find the range of geological deformation, and then the image matching based on the generalized orthophoto is used to find the displacement of the specific point, so as to realize the quantitative analysis of the deformation position.
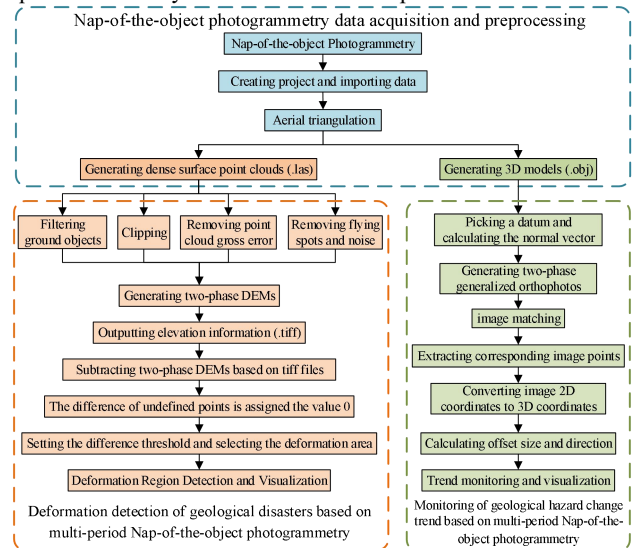
Figure 2. Technical route

3.1 Discovery of Geological Deformation Regions Based on DEM Difference Analysis

The deformation area can be found by subtracting the elevation values of the multi-period DEM data using the same datum plane, the formula is shown as (1).

$$\Delta h_{(i,j)} = DEM_{L_{(i,j)}} - DEM_{F_{(i,j)}},\qquad(1)$$

where $DEM_{L_{(i,j)}}$ = the DEM data for the new period

$DEM_{F_{(i,j)}}$ = the DEM data for the old period

(i, j) = the DEM data for the old period.

The principle is shown in Fig. 3.
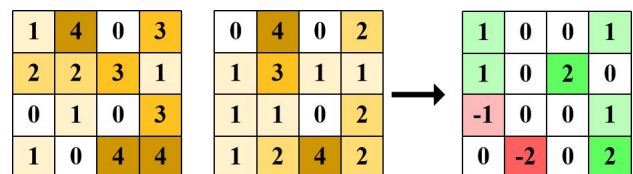
Figure 3. DEM difference analysis schematic diagram.

3.2 Geological Deformation Trend Based on Generalized orthophoto

After the significant deformation region of the geological disaster is discovered, in order to study the deformation trend of the geological disaster and calculate the size and direction of its displacement, it is necessary to produce multi-period generalized orthophotos suitable for high-precision Nap-of-the-object photogrammetry, and then match the orthopjotos, inversely calculate the three-dimensional coordinate system of the corresponding image points, and obtain the deformation of deformation trend.

3.2.1 Production of Generalized orthophoto

orthophoto refers to the image produced by vertical projection of the target region. However, the deformation caused by geological disasters, related to terrain fluctuations, slopes, etc.,

has significant arbitrariness in three-dimensional space. Generalized orthophoto produced by orthogonal projection of a plane of interest, which can describe geological deformation to the greatest extent.

Let the formula of the fitting plane be (2).

$$aX + bY + cZ = d \qquad (2)$$

Then the equation for solving the fitting plane is (3).

$$a(X_i - \overline{X}) + b(Y_i - \overline{Y}) + c(Z_i - \overline{Z}) = 0 (i = 1, 2, 3, 4), (3)$$

where (X_i, Y_i, Z_i) = three-dimensional object coordinates of four vertices
$(\overline{X}, \overline{Y}, \overline{Z})$ = average coordinates of four vertices.

Constraints can be expressed as $A\mathrm{X} = 0$, where A and X are (4).

$$A = \begin{pmatrix} X_1 - \overline{X} & Y_1 - \overline{Y} & Z_1 - \overline{Z} \\ X_2 - \overline{X} & Y_2 - \overline{Y} & Z_2 - \overline{Z} \\ X_3 - \overline{X} & Y_3 - \overline{Y} & Z_3 - \overline{Z} \\ X_4 - \overline{X} & Y_4 - \overline{Y} & Z_4 - \overline{Z} \end{pmatrix}, \mathrm{X} = \begin{pmatrix} a \\ b \\ c \end{pmatrix} \qquad (4)$$

To minimize the sum of distances, i.e.: $\min \|A\mathrm{X}\|$, singular value decomposition is performed on A, make $\|\mathrm{X}\| = 1$ as the constraint condition, and X can be solved.

After solving (a, b, c), in order to establish the geometric relationship between three-dimensional points and generalized orthophoto, let the origin of the three-dimensional point cloud coordinate system be O, the projection plane be λ, and the distance from O to λ be r (and let this line segment be γ). The positive angles between γ and each coordinate axis OX, OY, OZ of the three-dimensional object coordinate system $O - XYZ$ are α, β, ϕ respectively; the projection of γ on the XOY plane of the three-dimensional point cloud coordinate system is L, so the included angle of γ and L is $|\varphi - \pi/2|$, and the included angle of L and X axes is θ. The schematic diagram is shown in Fig. 4.
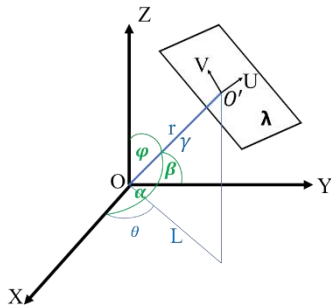
Figure 4. Coordinate transformation between 3D model coordinate system and 2D reference plane coordinate system.

Then there are (5).

$$\cos\alpha = \sin\varphi\cos\theta = \frac{a}{\sqrt{a^2 + b^2 + c^2}}$$

$$\cos\beta = \sin\varphi\sin\theta = \frac{b}{\sqrt{a^2 + b^2 + c^2}} \qquad (5)$$

$$\cos\varphi = \frac{c}{\sqrt{a^2 + b^2 + c^2}}$$

Let the origin of the two-dimensional plane be the vertical foot O' of γ in the plane λ, the coordinate axis are u, v respectively, the unit vector of $\overrightarrow{O'O}$ is $\overrightarrow{\ell_\lambda} = -(\cos\alpha, \cos\beta, \cos\varphi)$, and because of $\overrightarrow{O'O} \perp \lambda$, there are (6) and (7).

$$\overrightarrow{\ell_U} = \frac{1}{\sqrt{1-\cos^2\alpha}}\{\cos^2\varphi + \cos^2\beta, \ -\cos\alpha\cos\beta, \ -\cos\alpha\cos\varphi\}, (6)$$

$$\overrightarrow{\ell_V} = \frac{1}{\sqrt{1 - \cos^2\alpha}}\{0, \ -\cos\varphi, \ \cos\beta\}, \qquad (7)$$

The unit vector $\overrightarrow{\ell_U}$ and $\overrightarrow{\ell_V}$ can be calculated with the two-dimensional projection datum parameter (a, b, c), as in formulas (8) and (9).

$$\overrightarrow{\ell_U} = \frac{1}{\sqrt{(b^2 + c^2)(a^2 + b^2 + c^2)}}\{b^2 + c^2, \ -ab, \ -ac\} \qquad (8)$$

$$\overrightarrow{\ell_V} = \frac{1}{\sqrt{b^2 + c^2}}\{0, \ -c, \ b\} \qquad (9)$$

The coordinates of point O' in the three-dimensional object coordinate system are shown in formula (10).

$$O' = (r \cdot \cos\alpha, \ r \cdot \cos\beta, \ r \cdot \cos\phi) = \frac{r}{\sqrt{a^2 + b^2 + c^2}}(a \ \ b \ \ c) \qquad (10)$$

Then the projection coordinate O' of the three-dimensional point O' in the plane O' is as formula (11).

$$x' = \mathrm{Pr}\,j_U \overrightarrow{O'P} = \frac{\overrightarrow{O'P} \bullet \overrightarrow{\ell_U}}{|\overrightarrow{\ell_U}|} = \overrightarrow{O'P} \bullet \overrightarrow{\ell_U},$$

$$y' = \mathrm{Pr}\,j_V \overrightarrow{O'P} = \frac{\overrightarrow{O'P} \bullet \overrightarrow{\ell_V}}{|\overrightarrow{\ell_V}|} = \overrightarrow{O'P} \bullet \overrightarrow{\ell_V} \qquad (11)$$

which expands to formula (12).

$$x' = \frac{1}{\sqrt{(b^2 + c^2)(a^2 + b^2 + c^2)}}\left(X - r \cdot \frac{a}{\sqrt{a^2 + b^2 + c^2}} \quad Y - r \cdot \frac{b}{\sqrt{a^2 + b^2 + c^2}} \quad Z - r \cdot \frac{c}{\sqrt{a^2 + b^2 + c^2}}\right)\begin{pmatrix} b^2 + c^2 \\ -ab \\ -ac \end{pmatrix}$$

$$= \frac{X(b^2 + c^2) - Yab - Zac}{\sqrt{(b^2 + c^2)(a^2 + b^2 + c^2)}}$$

$$y' = \frac{1}{\sqrt{b^2 + c^2}}\left(X - r \cdot \frac{a}{\sqrt{a^2 + b^2 + c^2}} \quad Y - r \cdot \frac{b}{\sqrt{a^2 + b^2 + c^2}} \quad Z - r \cdot \frac{c}{\sqrt{a^2 + b^2 + c^2}}\right)\begin{pmatrix} 0 \\ -c \\ b \end{pmatrix}$$

$$= \frac{-Yc + Zb}{\sqrt{b^2 + c^2}}$$

(12)

In this way, the geometric relationship between the 3D point and the generalized orthophoto is established.

3.2.2 Calculation of Displacement Based on Corresponding Image Points

After producing the generalized orthophotos, the multi-period images are matched. In this paper, Harris is used to extract feature points, and then the Normalized Correlation Coefficient(NCC) is used for image matching to obtain corresponding image points of multi-period generalized orthophoto. The corresponding image points in the new and old periods are expressed as $P'_{L_i}\left(x'_{L_i}, \quad y'_{L_i}\right)$ and $P'_{F_i}\left(x'_{F_i}, \quad y'_{F_i}\right)$.

Through the inverse coordinate transformation of the 2D datum plane to the 3D object coordinates, and the constraints of the intersection of the projected baseline and the triangular element of the TIN mesh, the 3D object coordinates $P_{L_i}\left(X_{L_i}, \quad Y_{L_i}, \quad Z_{L_i}\right)$ and $P_{F_i}\left(X_{F_i}, \quad Y_{F_i}, \quad Z_{F_i}\right)$ of the object points in the old and new periods are obtained.

Then the displacement of the geological deformation trend of the object point is as (13).

$$
\begin{aligned}
dx &= X_{L_i} - X_{F_i} \\
dy &= Y_{L_i} - Y_{F_i} \\
dz &= Z_{L_i} - Z_{F_i}
\end{aligned}
\tag{13}
$$

4. EXPERIMENT AND CONCLUSION

4.1 Experimental Data and Processing Results

This paper takes the slope of Huangdeng Hydropower Station on the Lancang River as the research object. In September 2020 and September 2021, UAV Photogrammetry is used to obtain multi-period Nap-of-the-object images with resolutions of 0.015m and 0.025m respectively. 400-900 posted Nap-of images in both periods.

3DJI_0001.JPG   3DJI_0002.JPG   3DJI_0003.JPG

3DJI_0007.JPG   3DJI_0008.JPG   3DJI_0009.JPG

3DJI_0013.JPG   3DJI_0014.JPG   3DJI_0015.JPG
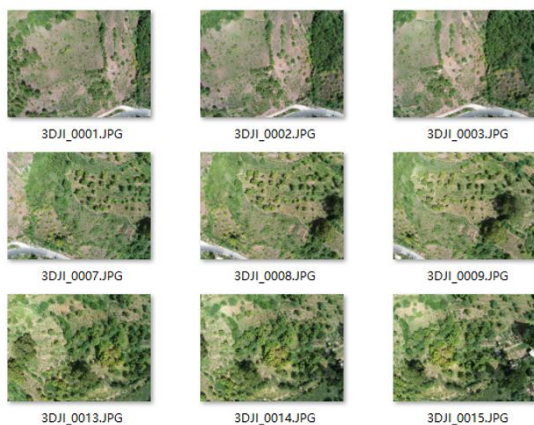
Figure 5. Nap-of-the-object image overview of the survey area.

After data preprocessing, the dense point cloud 3D model LAS of the target area and the refined 3D model OBJ are obtained, as shown in Fig. 6 and Fig. 7.

Figure 6. Refined 3D scene model overview.

Figure 7. Detailed display of the refined 3D scene model.

The DEM difference analysis results are shown in Fig.

$|D_H| > 3|D_Z|$

$3|D_Z| > |D_H| > 2|D_Z|$

$2|D_Z| > |D_H| > |D_Z|$

$|D_H| < |D_Z|$

8.
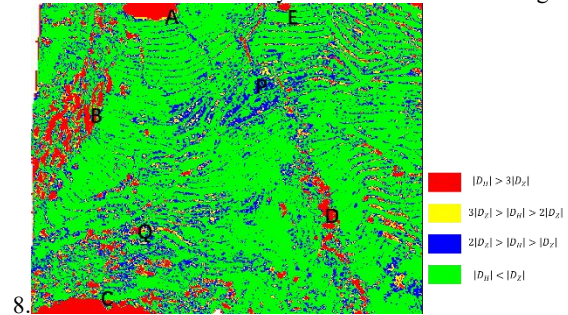
Figure 8. DEM difference analysis results.

The generalized orthophotos produced for the deformed region are shown in Fig. 9 and Fig.10.

Figure 9. Generalized orthophoto of deformed Regions of in 2020.

Figure 10. Generalized orthophoto of deformed Regions in 2021.

The results of obtaining corresponding image points based on multi-period generalized orthophoto matching are shown in Fig. 11.

Figure 11. Corresponding image points based on image matching

The displacement of geological deformation trend is shown in Fig. 12.

Figure 12. Displacement of deformation trend.

By extracting the coordinate information of corresponding image points, a total of 264 pairs of image can be obtained. The distance between the corresponding image points is calculated as the displacement $\vec{s_i} = \left(x'_{L_i} \quad y'_{L_i} \right) - \left(x'_{F_i} \quad y'_{F_i} \right)$, and the direction vector of the changing trend $\vec{n}$, then, arrange the displacement in ascending order, as shown in the Table 1.

x'_{F_i}/cm	y'_{F_i}/cm	x'_{L_i}/cm	y'_{L_i}/cm	$|\vec{s_i}|$/cm	$\vec{n}$/cm
232	258	230.05	257.89	1.96	(-0.998, -0.059)
461	198	460.70	195.81	2.21	(-0.136, -0.991)
824	527	823.52	524.79	2.27	(-0.214, -0.977)
344	162	345.67	160.17	2.47	(0.673, -0.740)
564	352	563.20	349.54	2.59	(-0.310, -0.951)
56	287	54.39	284.77	2.75	(-0.586, -0.810)
921	146	923.28	144.39	2.79	(0.816, -0.577)
831	237	830.33	234.23	2.85	(-0.235, -0.972)
784	197	783.18	194	3.11	(-0.263, -0.965)
217	205	215.28	202.18	3.30	(-0.521, -0.854)
136	197	133.85	199.62	3.39	(-0.636, 0.772)

Table 1. The magnitude and direction of the displacement.

To illustrate the effectiveness of the method proposed in this paper, we compared the monitoring results with the GNSS detection results, and the selected comparison points are shown in Figure 13.

Figure 13. Severely deformed area and GNSS calibration pile

We selected 5 GNSS calibration piles from the severely deformed area, and the true deformation values are shown in Table 2. We also randomly selected 20 model points around the calibration piles, and the deformation displacement is shown in Table 3.

dX/cm	dY/cm	dZ/cm	$|S|$/cm	$\overline{|s|}$/cm
16.77	23.23	-35.54	45.65	
17.64	24.44	-33.1	44.77	
27.34	9.80	-41.85	50.94	45.80
22.04	23.77	-32.8	46.12	
18.36	31.5	-19.19	41.54	

Table 2. Displacement of GNSS calibration piles

dX/cm	dY/cm	dZ/cm	$|S|$/cm	$\overline{|s|}$/cm
17.42	17.90	-43.76	50.39	
22.53	25.27	-44.89	56.23	
17.03	25.98	-40.74	51.23	
20.47	20.39	-35.62	45.86	
13.96	26.18	-39.03	49.02	
32.54	15.03	-21.15	41.62	
4.01	28.61	-42.72	51.57	
21.17	18.00	-32.65	42.88	
24.67	14.98	-35.58	45.81	
15.71	25.19	-30.90	42.85	46.76
17.90	20.63	-33.97	43.59	
24.36	14.11	-35.66	45.43	
14.46	23.27	-37.26	46.25	
9.91	32.11	-28.76	44.23	
25.33	10.38	-35.95	45.18	
13.38	23.69	-30.53	40.90	
8.83	32.51	-26.26	42.72	
23.63	22.64	-35.27	48.11	
13.55	31.79	-32.12	47.18	
3.86	31.08	-44.26	54.22	

Table 3. Displacement of Sampling model points

The deformation measured by GNSS calibration pile and Nap-of-the-object Photogrammetry are both about 45cm, and the deformation monitoring results are consistent, so the result shows that this method is very effective.

4.2 Conclusion

The technologies of geological disaster dynamic monitoring based on Nap-of-the-object photogrammetry were applied to the slope area where geological disasters frequently occur near Lancang River. The results show that the deformation area detection method proposed in this paper is simple and effective, which can quickly discover the deformation region. The deformation trend prediction based on multi-period generalized orthophoto is feasible, and the displacement with deformation of 3 cm can be accurately pointed out.
The algorithm used in this paper has more advantages in corner detection. In the future, the matching algorithm will be further improved, and detection methods for different terrain features and more suitable for surface feature points of a large range of geological hazards are proposed to achieve better matching effect.

5. ACKNOWLEDGEMENTS

REFERENCES

Li, H.M., 2019. Application of 3S Technology in Landslide Monitoring of Fushun West Open-pit Mine. Jilin University.

Zai, C.X., 2021. Research on the construction method of refined 3D model based on various photography methods. Kunming University of Science and Technology.

Zhang, G.Z., 2020. Research on Modeling Technology of High-precision 3D Real Scene Model in Urban Built-up Area. Anhui University of Science and Technology.

He, J.N., 2019. Nap-of-the-Object Photogrammetry and Its Key Techniques. Wuhan University.

Liang, J.T., Tie, Y.B., Zhao, C., Zhang, S., 2020. Technology and method research on the early detection of high-level collapse based on the nap-of-the-object photography. Geological Survey of China, 7(5), 107-113.

Yang, Y., Tao P.J., Zhong, L., Xu C.Y., 2020. Application of close photogrammetry technology in the supervision of the middle route of the South-to-North Water Diversion Project——Taking the Dengzhou section at the head of the canal as an example. CHES Ann. Water Resources and Hydropower Engineering., 360-363.

Li, Z.J., Zhong, L.T., Huang, Y.H., et al., 2021. Monitoring technology for collapse erosion based on the nap of the object photograph of UAV. Transactions of the Chinese Society of Agricultural Engineering (Transactions of the CSAE), 37(8), 151-189.

Zheng, S.Y., Su, G.Z., Zhang, Z.X., 2005. Automatic Reconstruction of 3D Surface Model with 3D Irregular Points Based on Projection Constrain. Geomatics and Information Science of Wuhan University, 2005(02):154-157.